Surface & Coatings Technology 391 (2020) 125683

Contents lists available at ScienceDirect

Surface & Coatings Technology

journal homepage: www.elsevier.com/locate/surfcoat

Mechanisms of particle ejection from free-standing two-layered graphene stimulated by keV argon gas cluster projectile bombardment – Molecular dynamics study

M. Gołuński*, S. Hrabar, Z. Postawa

Institute of Physics, Jagiellonian University, ul. Lojasiewicza 11, 30-348 Krakow, Poland

ARTICLE INFO

Keywords:
Graphene
Argon cluster
Molecular dynamics
SIMS

ABSTRACT

Molecular dynamics computer simulations are employed to investigate processes leading to particle ejection from free-standing two-layered graphene irradiated by keV argon gas cluster projectiles. The effect of the primary kinetic energy and the projectile size on the ejection process is investigated. It has been found that both these parameters have a pronounced influence on the emission of particles. The interaction between argon projectiles and graphene is strong regardless of graphene's minimal thickness. A significant portion of the primary kinetic energy is deposited into the sample. Part of this energy is used for particle emission, which is substantial. As a result, circular nanopores of various dimensions are created depending on the bombardment conditions. A major part of the deposited energy is also dispersed in a form of acoustic waves. Different mechanisms leading to particle ejection and defect formation are identified depending on the projectile energy per atom. The implications of the results to a novel analytical approach in Secondary Ion Mass Spectrometry based on ultrathin free-standing graphene substrates and a transmission geometry are discussed.

1. Introduction

Two-dimensional crystals have been a subject of extensive studies for some time due to their unique properties [1]. One of the most inspiring 2D materials is graphene. Due to its exceptional electric properties, high intrinsic strength, and stiffness, this material entered many fields of engineering, for example electronics, composite materials, and photovoltaics, just to name a few [2,3]. Despite the already conducted extensive studies, still much effort must be spent to better understand various aspects of graphene and graphene-like materials [4].

There are numerous methods used for graphene preparation, characterization, or alteration. Some of them are relying on ion beam bombardment [5]. Two of the less apparent forms of using the ion beam are cleaning the graphene surface from contaminations and uplifting of deposited material for further chemical analysis. Kim et al. considered the cleaning of suspended graphene with argon clusters [6], while few others worked on the subject of using these projectiles for cleaning of graphene supported on the surface [7–10]. Verkhoturov et al. proposed to use free-standing graphene as a substrate for chemical analysis by Secondary Ion Mass Spectrometry (SIMS). In this approach, a so-called "transmission geometry" is used in which the analysed organic material is deposited on one side of the ultrathin substrate, while another side is bombarded by cluster projectiles [11,12]. It is argued that such geometry can be particularly attractive for the analysis of ultra-small amounts of organic material, molecular nano-objects, and supramolecular assemblies [11,12].

Cluster ion beams are a natural choice to uplift the organic molecules. Impacts of these projectiles lead to more gentle, collective movement of the substrate and analysed material, which favours the emission of intact molecules [13,14]. Although one of the most successful clusters used in organic SIMS is C_{60} fullerene [15], there is a significant movement towards larger clusters, such as argon gas clusters consisting of hundreds or even thousands atoms [16–18]. Bombardment of free-standing graphene by C_{60} projectiles has already been investigated [11,19–24]. However, there is no analogous work available for larger clusters, even though these projectiles are more optimal for the analysis of materials consisting of large organic molecules [13,14]. As a result, not much is known about processes that will lead to a material ejection in this case. Most of the existing theoretical works on the projectile-graphene interaction focuses on the ion beam-induced creation of defects in graphene [25,26]. Much less is known about processes that cause removal of carbon atoms from this material,

---

Abbreviations: MD, molecular dynamics; SIMS, Secondary Ion Mass Spectrometry

* Corresponding author at: ul. Lojasiewicza 11, 30-348 Krakow, Poland.

E-mail addresses: mikolaj.golunski@gmail.com (M. Gołuński), sviatoslav.hrabar@doctoral.uj.edu.pl (S. Hrabar), zbigniew.postawa@uj.edu.pl (Z. Postawa).

https://doi.org/10.1016/j.surfcoat.2020.125683
Received 17 November 2019; Received in revised form 21 February 2020; Accepted 23 March 2020

leading to creation of defects, particularly when large cluster projectiles are used. The objective of this paper is, therefore, to describe the dynamics of the energetic argon gas cluster bombardment of free-standing graphene. The results are used to provide insight into phenomena leading to the ejection of atoms from the bombarded system.

2. Computer model

The molecular dynamics (MD) computer simulations are used to model cluster bombardment. Briefly, the movement of particles is determined by integrating Hamilton's equations of motion. The forces between carbon atoms in the system are described by the Charge Implicit ReaxFF (CI-ReaxFF) force field [27], which allows for the creation and breaking of covalent bonds. While preserving the accuracy of the original ReaxFF potential, this force field is several times faster and has an appropriate repulsive wall to describe high energy collisions properly. Forces between argon atoms and between argon and carbon atoms are described by the Lenard-Jones potential [28] splined with KrC potential [29] for high energy collisions. A more detailed description of the MD method can be found elsewhere [30]. The gas clusters consisting of 60, 100, 366, and 1000 argon atoms are chosen as projectiles. These clusters have diameters of approximately 1.4 nm, 1.6 nm, 3 nm, and 4 nm, respectively. The kinetic energy and number of argon atoms in the projectile cluster are changed to investigate the effect of these parameters on the particle ejection process. Impacts of Ar_{60}, Ar_{100}, Ar_{366}, and Ar_{1000} projectiles with kinetic energy between 1 and 40 keV are investigated. All impacts occur along the surface normal. The shape and size of the samples are chosen based on visual observations of energy transfer pathways stimulated by the impacts of argon clusters. As a result, cylindrical samples are used. For Ar_{60}, Ar_{100}, and Ar_{366} projectiles samples have a diameter of 40 nm. Substrates with a diameter of 80 nm are used for the Ar_{1000} projectile. Samples consist of a double layer of graphene with a highly oriented pyrolytic graphite structure. They contain 92,126 and 368,564 atoms, respectively. Rigid and stochastic regions are used to simulate the thermal bath that keeps the sample at the required temperature, to prevent reflection of pressure waves from the boundaries of the system, and to maintain the shape of the sample [30,31]. The simulations are run at a target temperature of 0 K. Most simulations extend up to 10 ps, which is long enough to achieve saturation in the ejection yield versus time dependence. Only simulations for Ar_{1000} with kinetic energy below 15 keV are run for 80 ps to investigate the massive deformation of graphene, which occurs in these systems over a prolonged time. Twenty-five impact points randomly selected near the centre of the sample are chosen for each combination of projectile size and primary kinetic energy to achieve statistically reliable data. Simulations are performed with the large-scale atomic/molecular massively parallel simulator code (LAMMPS) [32], which has been modified to describe sputtering conditions better. In principle, particles ejected in the direction of the primary beam (the transmission direction) and in the opposite direction (the reflection direction) are collected. However, as emission in the reflection direction is minimal, only the data for the transmission direction are presented in this paper.

3. Results and discussion

Dependence of the total sputtering yield and of the fraction of projectile atoms penetrating through the sample on the primary kinetic energy is presented in Fig. 1. The yield initially increases with kinetic energy but saturates for higher energies in the investigated range for the same projectile. For each projectile, there is a minimum kinetic energy required to eject substrate particles or to perforate graphene. These energies are presented in Table 1. Threshold energy shifts towards larger values with the projectile size. Furthermore, the ejection of graphene atoms requires higher kinetic energy than the emission of argon atoms. The latter is an indicator of graphene perforation. Difference between these two thresholds increases with the projectile size. This means that it is easier for a large projectile to penetrate graphene without emission of carbon atoms.

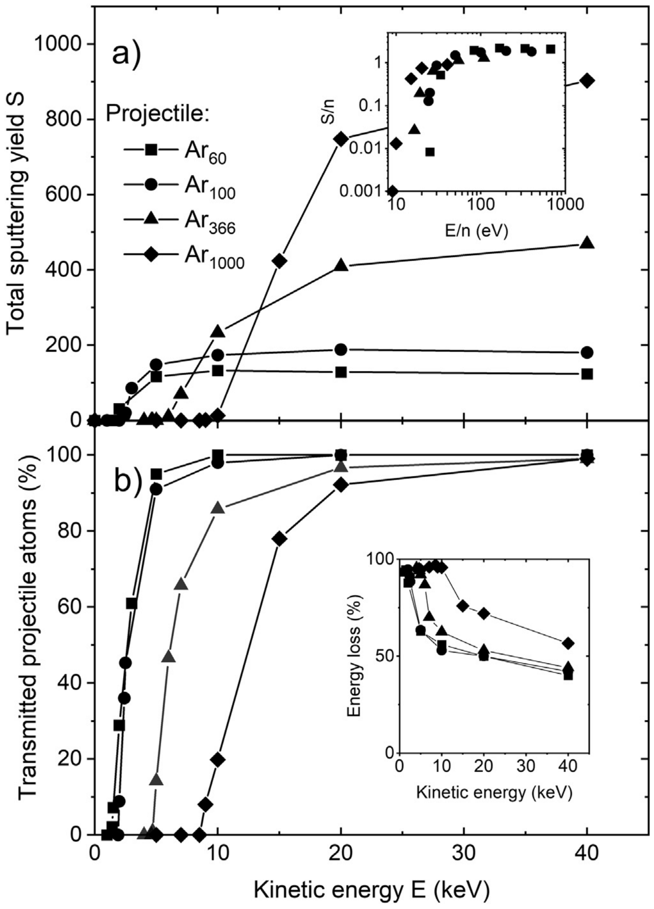

Fig. 1. The effect of the projectile kinetic energy E and size n on a) sputtering yield S, and b) fraction of transmitted projectile atoms for various Ar clusters. The inset to panel a) shows the data normalized to the number of projectile atoms. The inset to panel b) shows the fraction of the primary kinetic energy lost by the projectile.

Table 1
Values of the threshold energy E_{th}, threshold energy per atom E_{th}/n, threshold momentum (M_{th}), and threshold projected momentum M_{pth} for substrate particle emission (_s) and graphene perforation (_p).

	Ar_{60}	Ar_{100}	Ar_{366}	Ar_{1000}
E_{th_s} (keV)	1.5	2.4	5.0	10.0
E_{th_p} (keV)	1.4	2.0	4.7	9.0
E_{th_s}/n (eV)	25	24	13	10
E_{th_p}/n (eV)	23	20	12	9
M_{th_s} (kg * m/s) * 10^{-19}	0.6	1.0	2.8	6.5
M_{th_p} (kg * m/s) * 10^{-19}	0.6	0.9	2.7	6.2
M_{pth_s} (kg * m/s/m^2) * 10^2	4.0	5.0	3.9	5.2
M_{pth_p} (kg * m/s/m^2) * 10^2	3.9	4.6	3.8	4.9

It has been shown that the relation between the sputtering yield S and parameters of the cluster projectiles can be significantly simplified if the data are presented in a special form [33–35]. Such representation, sometimes called "universal", is shown in the inset to Fig. 1a [33,34]. Indeed, at the high E/n region, data points for all projectiles are located at the same line, and the dependence between S/n and E/n is linear, where E is the projectile's kinetic energy, and n is the number of projectile atoms. At low E/n value, the data points cannot be placed on a single line, and the S/n vs E/n dependence becomes nonlinear, as reported previously [33,34]. The onset of the nonlinear region depends strongly on the cluster size, shifting it to the lower kinetic energy per atom as the size of the cluster projectile increases. The same trend has been observed previously [33,34]. Our results indicate that the universal representation implemented for the sputtering of thick samples is valid also for systems with limited dimensionality. Popok et al. [35] proposed another approach aimed at simplifying the relation between projectile range and projectile parameters. In this approach, the effect of projectile size and its kinetic energy was unified by using the projectile momentum [35]. The effect of the application of all these approaches to our threshold energy data is shown in Table 1. It is evident that expressing the ejection onsets by the projected momentum seems to be the most universal. The projected momentum is calculated by dividing the projectile momentum by the area of the projectile's projection on the graphene surface, as proposed in Ref. [35].

The yield of ejected carbon atoms increases with the projectile size when the primary kinetic energy is constant. There is a significant particle emission from the bombarded sample, especially for large high-energy projectiles. Almost all projectile atoms penetrate through an ultrathin sample. Only below approximately 5 keV for Ar_{60}, $Ar_{100,}$ 10 keV for Ar_{366}, and 15 keV for Ar_{1000} penetration efficiencies are significantly reduced, as shown in Fig. 1b. It is evident that a significant fraction of the primary kinetic energy is lost by a projectile regardless of the minimum thickness of the sample, as indicated by the data presented in the inset to Fig. 1b. For instance, for 10 keV projectiles, more than half of the primary kinetic energy is lost when penetrating through graphene layers. This fraction decreases as the kinetic energy increases for a given projectile size. It also increases as the projectile size decreases for a given primary kinetic energy, particularly at low kinetic energy. It is interesting to note that the projectile loses its kinetic energy even in cases where no ejection of substrate atoms occurs. This observation indicates that graphene sheets consume a part of the primary kinetic energy.

The primary kinetic energy also influences the relative contribution of various species in the ejected plum, as presented in Fig. 2. Numbers in the bottom-right corners of individual spectra indicate the kinetic energy per projectile atom, which is proposed as the universal metric to characterize ejection phenomena stimulated by cluster projectile impacts [33,34]. This quantity is proportional to a square of the projectile velocity. For energetic projectiles, mainly carbon monomers populate the plum. The most abundant ejection shifts to larger fragments with a decrease of the projectile energy per atom. At the same time, a relative ejection of carbon monomers decreases. At certain conditions, carbon trimers are the most abundant species in the ejected flux, as seen, for instance, for 20 and 40 keV Ar_{1000} projectiles (20 and 40 eV/n respectively). For these impacts, the emission of carbon monomers is almost absent. This is a surprising observation, as in a typical sputtering experiment the emission of monomers is a dominant channel of particle removal [36]. Based on the similarities in the mass spectra, we divide all investigated impacts into three categories, as indicated in Fig. 2. Impacts leading to the significant ejection of carbon monomers are classified as category A. This category contains impacts of the projectiles with the largest kinetic energy per atom used in our study. Impacts leading to a dominant emission of larger fragments are marked as category B. This category includes medium energy impacts. Finally, impacts resulting in no emission of substrate particles are grouped in category C. This category contains impacts of the projectiles with the lowest kinetic energy per atom investigated in our study.

Differences in the particle emission process caused by impacts assigned to categories A, B, and C are even more pronounced in velocity distributions of the ejecta. In Fig. 3, we present velocity distributions of C, C_2, and C_3 fragments ejected from graphene in the transmission direction. The spectra are normalized to their maxima, because in the following reasoning we will be interested only in their shape. For category A impacts, the ejecta have broad velocity distributions. The shape and the peak position of spectra for each fragment type are different. Carbon monomers are, on average, the fastest-moving particles. Larger fragments move with lower velocity, which is typical behaviour observed for sputtering experiments [36]. Much more interesting are the velocity spectra of particles ejected by impacts classified as category B. These spectra are narrower than earlier distributions. Surprisingly, they have almost identical shapes for all three types of the emitted species at the same impact conditions. Moreover, the velocity corresponding to the most abundant emission correlates with the initial velocity of a projectile. These features are different from a typical

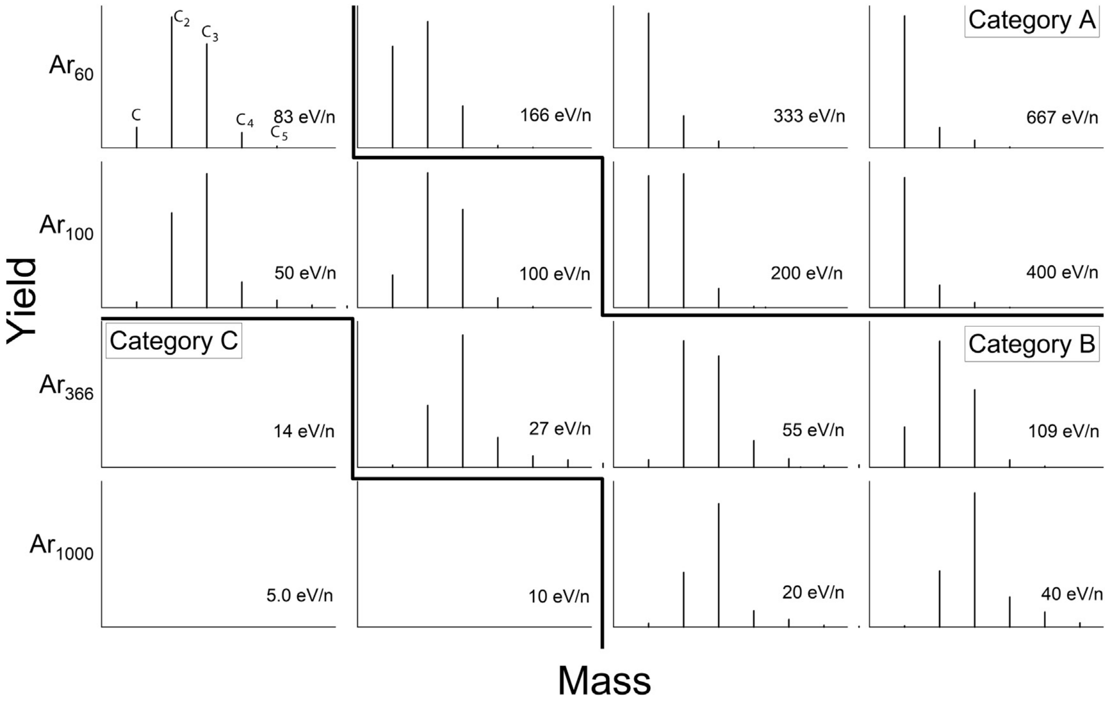

Fig. 2. Mass spectra of particles ejected in the transmission direction for 16 impact conditions corresponding to 4 projectile sizes and 4 primary kinetic energies. Graphs are grouped into three categories A, B, and C based on similarities of the spectra features (see text). Projectile atoms are not shown.

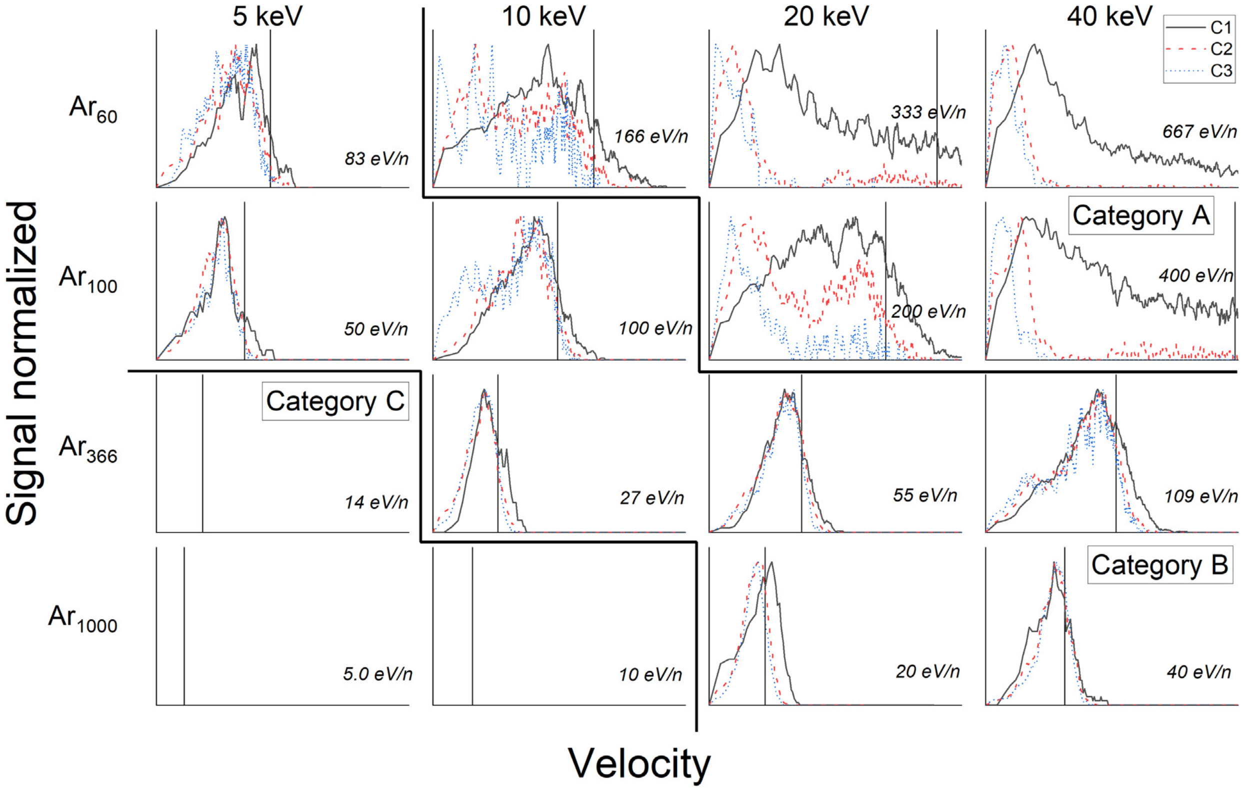

Fig. 3. Velocity distributions of 16 incidence conditions corresponding to different projectiles and primary kinetic energies. Different lines show velocities distributions of emitted C atoms (black solid line), C dimers (red dashed line), and C trimers (blue dotted line). Vertical lines denote the initial velocity of a projectile. All spectra are normalized to their maxima. Initial projectile velocity for the 40 keV Ar_{60} impact is outside of the velocity scale. Numbers at the bottom right corner of each spectrum depict the kinetic energy per projectile atom. (For interpretation of the references to colour in this figure legend, the reader is referred to the web version of this article.)

sputtering experiment, where the shape of the velocity spectra does not depend on the primary kinetic energy, at least in the linear cascade regime, and are usually different for various ejected species [36]. These differences can be expected, as there is no time and space for the linear collision cascade to develop in our samples. Nevertheless, the ejection of various fragments with the same velocity spectra is still puzzling. There are no velocity distributions in Fig. 3 for the impacts of category C, as no particles are ejected in this case.

The temporal evolution of studied systems is investigated to identify processes responsible for the particle ejection and explain the observed trends. The results are shown in Figs. 4, 5, 6, 7, and 8, as well as in Animations 1, 2, 3, and 4. An example of temporal snapshots for category A impacts is shown in Fig. 4, and in Animation 1. The data are obtained for 40 keV Ar_{60} projectile, which is the fastest projectile investigated in our study. The integrity of the projectile is compromised almost immediately after it passes through the graphene. However, during the impact, the projectile atoms stay together and interact collectively with the sample. After the collision, all projectile atoms penetrate through the substrate. The ejection of both projectile and substrate atoms is forward directed. Only a few substrate atoms are emitted

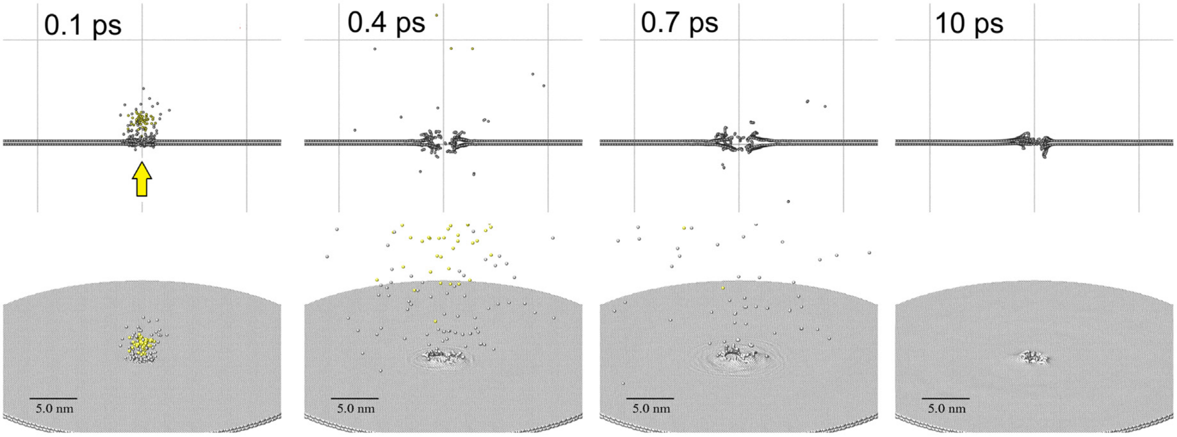

Fig. 4. Temporal snapshots from the simulation of a 40 keV Ar_{60} impact at graphene. The top row contains side views of the system obtained at various moments given by the values at the top left corners. The lower row contains perspective view of the same system. For a side view only 2 nm thick slice through the centre of the sample is shown. Carbon atoms are depicted as grey balls while argon atoms are yellow. Thin lines in the background denote the distance of 10 nm. Arrow indicates the direction of an incoming projectile. (For interpretation of the references to colour in this figure legend, the reader is referred to the web version of this article.)

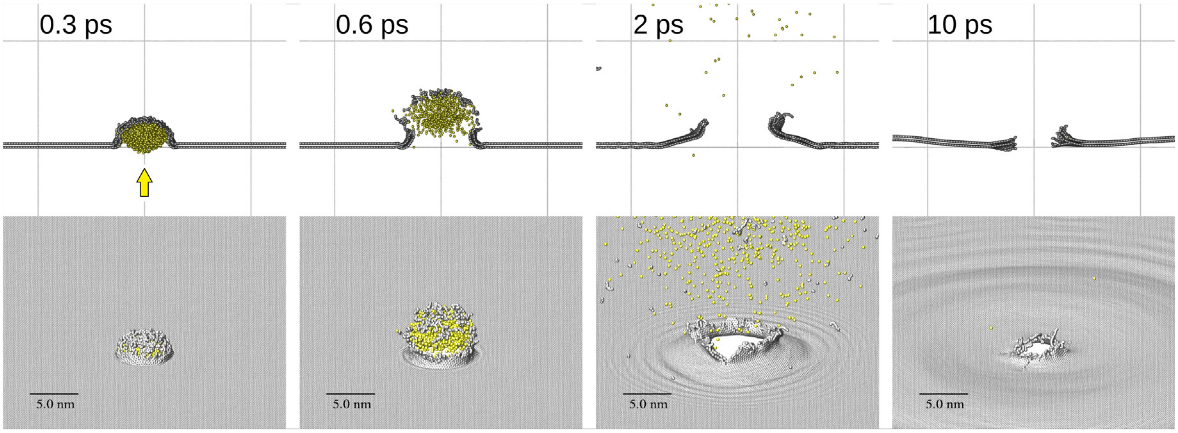

Fig. 5. Temporal snapshots from the simulation of a 40 keV Ar_{1000} impact at graphene. A detailed description of the content of the figure is provided in Fig. 4.

in the reflection direction. Atom removal leads to a formation of initially almost circular nanopore. Zhao et al. have found that energetic clusters can be used to fabricate nanopores in graphene in a controlled way by varying the properties of the incident beam [20,37]. They have found that impact energy of 11.4 eV per projectile atom is needed to create a nanopore in a single layer of graphene when bombarded with C_{60} projectile at normal incidence [20,37]. This value is smaller than the threshold energy for the nanopore formation by Ar_{60} projectiles, as shown in Table 1. This difference is expected, as Ar_{60} has a different mass than C_{60}, and two-layered graphene is bombarded in our case.

The structure of a newly created nanopore is dynamic. We observe, for instance, that new bonds are created in this area. The radicals created by the impact are highly reactive and tend to form new bonds instantly. Some of these bonds are also formed between carbon atoms located in different layers. Again, similar behaviour was reported for C_{60} bombardment of graphene [20,37], and C_{60} and Ar_n bombardment of fullerite [38]. These new bonds lead not only to a hardening of the rim but also to a partial self-healing of the created nanopore.

As already discussed, a significant fraction of the primary kinetic energy is transferred to the sample. Most of this energy is carried away by circular acoustic waves that propagate outward from the point of impact. For the Ar_{60} bombardment, these waves have a maximum amplitude of approximately 0.1 nm. The process is very effective as graphene planes can efficiently transfer kinetic energy. It has been shown, for instance, that this property is responsible for an unusually small sputtering yield observed from pyrolytic graphite bombarded by C_{60} [39].

The analysis of Animation 1 indicates that two processes lead to the emission of carbon particles. Initially, carbon atoms are ejected by a direct interaction with a projectile. Because the projectile is energetic, the collisions are violent, and a lot of energy is transferred between Ar and C atoms. Original bonds between carbon atoms are easily broken, which leads predominantly to the emission of monomers. The presence of a conglomerate of Ar and C atoms at a distance of ~1.5 nm from the graphene already at 100 fs, as seen in Fig. 4, indicates that most of the carbon atoms ejected in this phase have high velocities. The second process leading to particle ejection occurs later and may last for several picoseconds. The rim is energized during projectile penetration. Some of this energy can be used to eject carbon particles. These particles are ejected along various polar angles with lower kinetic energy than atoms emitted by a direct interaction with the projectile. However, there is also a significant vertical and radial movement in this area. The vertical movement initially leads to a temporary separation of the layers near the rim area. It has been shown that this process can be used to stimulate efficient emission of intact organic molecules from layers deposited on graphene substrate [12,24]. Later, the vertical movement combines with correlated radial displacements of C atoms around the rupture and is transformed into collective movements, which develop wave-like vertical oscillations and radial planar compressions. A similar phenomenon also has been observed on graphite and graphene surfaces bombarded by C_{60} [12,21,40,42]. Approximately 20% of the primary kinetic energy transferred from the projectile to the sample is carried away by ejected substrate atoms for a 40 keV Ar_{60} bombardment. The remaining part is carried away by outwardly propagating waves.

The projectile has a lower kinetic energy per atom during category B impacts as compared to the category A bombardment, as shown in Fig. 3. It means that it moves slower. Examples of category B impacts are presented in Fig. 5 (Animation 2) and in Fig. 6 for a 40 keV Ar_{1000}

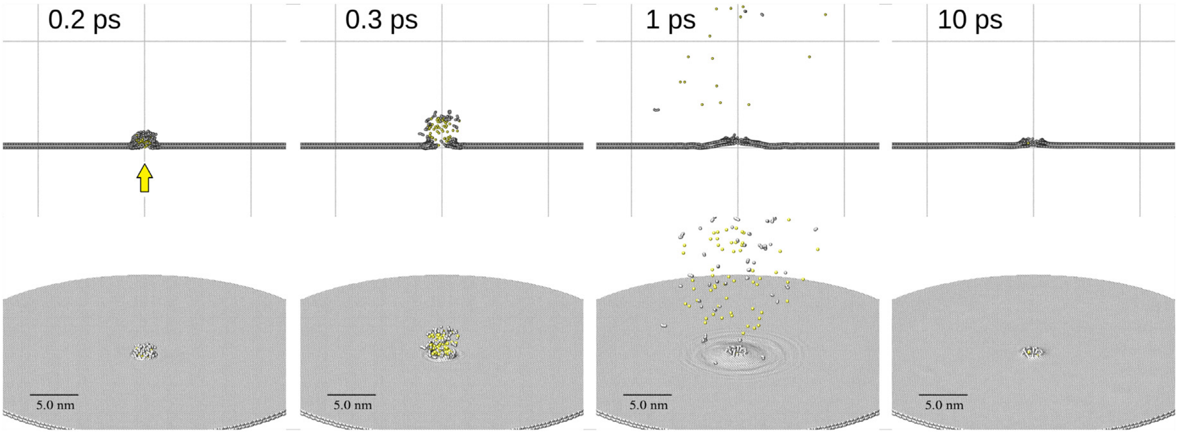

Fig. 6. Temporal snapshots from the simulation of a 5 keV Ar_{60} impact at graphene. A detailed description of the content of the figure is provided in Fig. 4.

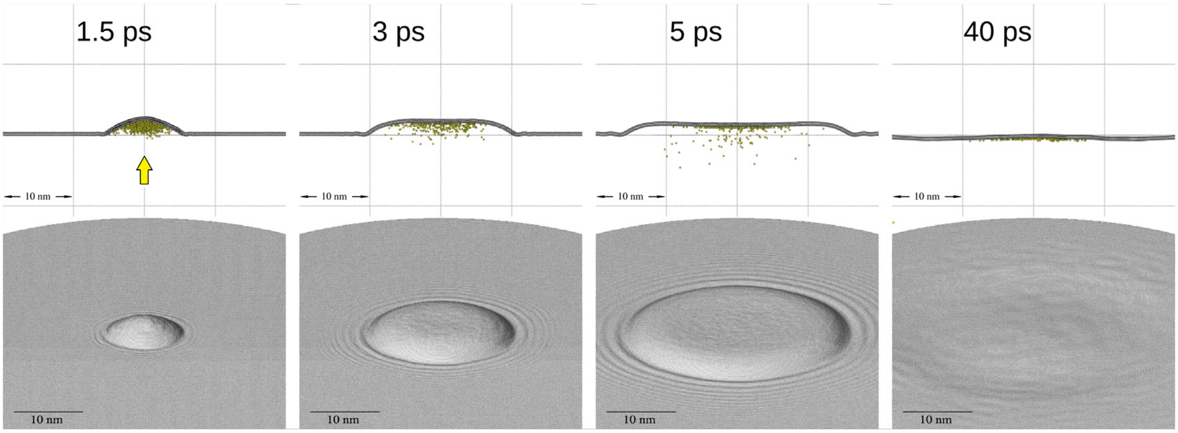

Fig. 7. Temporal snapshots from the simulation of a 5 keV Ar_{1000} impact at graphene. A detailed description of the content of the figure is provided in Fig. 4.

and 5 keV Ar_{60}, respectively. Just like in the case of category A impacts, projectiles are being compressed and flattened. However, the extent of flattening is more significant now. After approximately 0.2 ps for 5 keV Ar_{60} and 0.4 ps for 40 keV Ar_{1000} graphene becomes perforated. A large pore is formed for Ar_{1000}. However, even for 5 keV Ar_{60} projectiles, the orifice has a larger diameter as compared to the 40 keV Ar_{60} impact, as the 5 keV Ar_{60} projectile expands laterally before penetrating through the graphene layers. As shown in Figs. 5 and 6, and in Animation 2, carbon atoms located initially directly above the impinging projectile are removed collectively from the sample. They remain in almost original lattice, as they are entrained as one entity by Ar projectiles. Consequently, these atoms have similar velocities as the propagating clusters. This velocity is lower than the initial projectile velocity because a part of the primary kinetic energy is already consumed to perforate graphene. Carbon atoms entrained by the projectile are separated later when the projectile disintegrates, forming various fragments. However, they preserve their velocities. This observation explains why these particles have similar velocity distributions. Furthermore, the process is gentle and spatially correlated. Consequently, not only monomers but mostly larger fragments of the original lattice survive the ejection process. As a result, the peak in the mass spectra shifts towards larger fragments as compared to the mass spectra of category A impacts. The effect becomes more pronounced for larger projectiles. These observations account for the main features of the data shown in Figs. 2 and 3. Just like in the case of category A impacts, a fraction of the primary kinetic energy is deposited in graphene sheets, which leads to a formation of acoustic waves. Because the projectile is moving slower, there is more time for interactions between projectile atoms and atoms residing near the rim of the formed nanopore. More energy is transferred from the projectile to the sample. However, there is also more time to drain this energy away from the nanopore. Simulations indicate that this process is fast. Consequently, more acoustic waves with higher amplitudes are created, but the density of the deposited energy near the rim area is small. As a result, the rim is less energized, fewer carbon particles are emitted from this area, and carbon entrainment becomes the primary mechanism of particle ejection.

Finally, the impacts of category C should be discussed. These impacts do not lead to carbon ejection from the sample. However, graphene is still disturbed. In fact, the substrate can be more significantly altered than in previously discussed cases for the impacts of large projectiles. Our simulations identify two possible scenarios. In the first case, both the projectile momentum and its kinetic energy are not sufficient to perforate the sample. This scenario is illustrated in Fig. 7 and in Animation 3 for 5 keV Ar_{1000}. For these impact conditions, the projectile is almost entirely decelerated. During deceleration, projectile flattens significantly spreading its atoms over a wide area below the graphene. Most of the primary kinetic energy is transferred to the sample, as shown in Fig. 1. This energy is used predominantly to deform the sample and to create acoustic waves. As a result, the graphene surface bulges out in the direction of the primary beam over a large area, and numerous acoustic waves propagate outwards. Finally, the projectile atoms become back-reflected, but their kinetic energy is small. The deposited energy is carried away from the impact area and its density is not sufficient to stimulate the ejection of carbon from graphene. After the deposited energy is dispersed in graphene, the system returns to its initial shape.

In the second scenario, the momentum of the projectile is sufficient

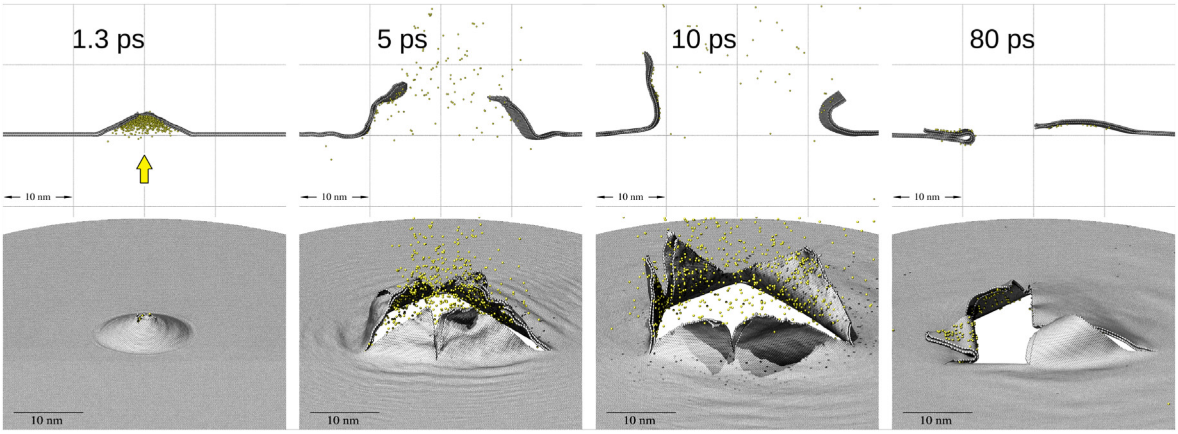

Fig. 8. Temporal snapshots from the simulation of a 10 keV Ar_{1000} impact at graphene. A detailed description of the content of the figure is provided in Fig. 4.

to break graphene, but the deposited density of the primary kinetic energy is still not enough to eject carbon atoms. This scenario is illustrated in Fig. 8 and in Animation 4 for a 10 keV Ar_{1000} impact. After the impact of a massive projectile, the graphene substrate begins to deform conically, just like it did in the earlier case. Graphene begins to buckle out. Again, the projectile decelerates and flattens over a large area. However, now its momentum is sufficient to rip the sample. A small rupture is formed initially, but soon radial cracks along crystallographic directions occur, which propagate quickly. Graphene layers unfold in a petal-like form. Five triangular-shaped petals fold at their bases. The system opens like a flower. The opening is vast, with dimensions significantly exceeding the projectile diameter. Argon atoms easily move through this opening. Individual petals move out. Some of them are even placed for a short moment on the graphene surface. Even in these extreme conditions, the structure does not break. Instead, the elastic strain forces the petals to move back into the opening. Even at the end of our simulation (80 ps) there is still kinetic energy in the petal movement. The formation of petal-like structures has also been shown in experiments with a supersonic micro-particle bombardment of multilayer graphene [43]. It is fascinating to note that even argon cluster projectiles can stimulate the same effects as orders of magnitude larger micro-projectiles. As indicated by Figs. 7 and 8, the processes stimulated by category C impacts are much more prolonged in time, as compared to scenarios present during category A and B impacts.

4. Conclusions

We presented the results of computer simulations investigating the bombardment of two-layered free-standing graphene by argon cluster projectiles with various kinetic energy and size. For most of the impacts considered, there is a substantial emission of carbon from graphene. Even though graphene is a very thin material, it absorbs a lot of the projectile's kinetic energy. Based on the differences in the ejecta, we divided impacts into three categories. Impacts with high kinetic energy per atom are described as category A. These impacts result in the ejection of high amounts of atomic carbon due to direct collisions with a projectile followed by emission from the energized rim of the rupture in graphene. Medium kinetic energy per atom impacts are classified as category B. In these impacts, the projectile gently pushes material out from graphene, resulting in the ejection of larger graphene fragments, especially C_3 particles. Finally, low-kinetic energy per atom impacts are described as category C. Such impacts do not lead to any carbon ejection even if they result in piercing the graphene layers. These impacts may, however, significantly modify a structure of graphene, especially for massive and large projectiles. In this case, the formation of large petal-like defects is observed. Similar structures have been already observed in experiments with micro-sized projectiles of comparable velocity and multilayer graphene targets [43].

It has been proposed that C_{60} projectiles can be used for a controlled perforation of graphene. In principle, also Ar clusters could be used for the same purpose as there is a definite relation between Ar cluster size and dimension of the nanopore created by its impact. From a practical point, however, it is currently not possible to make an ion beam composed of Ar clusters of the same size. Due to technical reasons, Ar ion beams always contain a distribution of Ar clusters with different sizes. As a result, only limited control of the pore sizes can be achieved with these projectiles.

Finally, a few comments can be made about the applicability of Ar cluster projectiles and ultrathin graphene substrates for SIMS analysis of organic overlayers in transmission geometry. Studies with C_{60} projectiles have shown that intact organic molecules are emitted by the unfolding of the topmost graphene layer. In this case, the graphene sheet acts as a catapult that can gently hurl molecules into the vacuum. There is a considerable amount of energy associated with this movement, which means that even very large molecules can be uplifted. During argon cluster bombardment, there is more energy in this motion, and the movement extends to a much higher lateral distance from the point of impact. Consequently, a larger number of adsorbed molecules could be ejected by a single projectile impact, making analysis of small amounts of organic material even more viable.

Supplementary data to this article can be found online at https://doi.org/10.1016/j.surfcoat.2020.125683.

Author statement

Mikołaj Gołuński: Conceptualization, Methodology, Validation, Formal analysis, Investigation, Data Curation, Writing - Original Draft, Writing - Review & Editing, Project administration, Funding acquisition.

Sviatoslav Hrabar: Data Curation, Visualization.

Zbigniew Postawa: Conceptualization, Software, Validation, Investigation, Resources, Writing - Review & Editing, Supervision, Funding acquisition.

Declaration of competing interest

The authors declare that they have no known competing financial interests or personal relationships that could have appeared to influence the work reported in this paper.

Acknowledgements

This work was supported by the National Science Centre, Poland grant numbers: 2016/23/N/ST4/00971 and 2015/19/B/ST4/01892. MD simulations were performed at the PLGrid Infrastructure, Poland.

References

[1] I. Lyuksyutov, A.G. Naumovets, V. Pokrovsky, Introduction, in: I. Lyuksyutov, A.G. Naumovets, V. Pokrovsky (Eds.), Two-dimensional Crystals, Academic Press, 1992, pp. 11–14.
[2] A.K. Geim, K.S. Novoselov, Nat. Mater. 6 (2007) 183–191.
[3] F. Bonaccorso, L. Colombo, G. Yu, M. Stoller, V. Tozzini, A.C. Ferrari, R.S. Ruoff, V. Pellegrini, Science 347 (2015) 1246501.
[4] A.C. Ferrari, F. Bonaccorso, V. Fal'ko, K.S. Novoselov, S. Roche, P. Boggild, S. Borini, F.H. Koppens, V. Palermo, N. Pugno, J.A. Garrido, R. Sordan, A. Bianco, L. Ballerini, M. Prato, E. Lidorikis, J. Kivioja, C. Marinelli, T. Ryhanen, A. Morpurgo, J.N. Coleman, V. Nicolosi, L. Colombo, A. Fert, M. Garcia-Hernandez, A. Bachtold, G.F. Schneider, F. Guinea, C. Dekker, M. Barbone, Z. Sun, C. Galiotis, A.N. Grigorenko, G. Konstantatos, A. Kis, M. Katsnelson, L. Vandersypen, A. Loiseau, V. Morandi, D. Neumaier, E. Treossi, V. Pellegrini, M. Polini, A. Tredicucci, G.M. Williams, B.H. Hong, J.H. Ahn, J.M. Kim, H. Zirath, B.J. van Wees, H. van der Zant, L. Occhipinti, A. Di Matteo, I.A. Kinloch, T. Seyller, E. Quesnel, X. Feng, K. Teo, N. Rupesinghe, P. Hakonen, S.R. Neil, Q. Tannock, T. Lofwander, J. Kinaret, Nanoscale 7 (2015) 4598–4810.
[5] S. Shukla, S.-Y. Kang, S. Saxena, Appl. Phys. Rev. 6 (2019) 021311.
[6] S. Kim, A.V. Ievlev, J. Jakowski, I.V. Vlassiouk, X.H. Sang, C. Brown, O. Dyck, R.R. Unocic, S.V. Kalinin, A. Belianinov, B.G. Sumpter, S. Jesse, O.S. Ovchinnikova, Carbon 131 (2018) 142–148.
[7] B.J. Tyler, B. Brennan, H. Stec, T. Patel, L. Hao, I.S. Gilmore, A.J. Pollard, J. Phys. Chem. C 119 (2015) 17836–17841.
[8] K. Mochiji, N. Inui, R. Asa, K. Moritani, E-Journal of Surface Science and Nanotechnology 13 (2015) 167–173.
[9] A.Y. Galashev, Comput. Mater. Sci. 98 (2015) 123–128.
[10] K. Moritani, S. Houzumi, K. Takeshima, N. Toyoda, K. Mochiji, J. Phys. Chem. C 112 (2008) 11357–11362.
[11] S. Geng, S.V. Verkhoturov, M.J. Eller, S. Della-Negra, E.A. Schweikert, J. Chem. Phys. 146 (2017) 054305.
[12] S.V. Verkhoturov, M. Gołuński, D.S. Verkhoturov, B. Czerwinski, M.J. Eller, S. Geng, Z. Postawa, E.A. Schweikert, J. Chem. Phys. 150 (2019) 160901.
[13] S. Fearn, Mater. Sci. Technol. 31 (2015) 148–161.
[14] N. Winograd, Gas cluster ion beams for secondary ion mass spectrometry, in: P.W. Bohn, J.E. Pemberton (Eds.), Annual Review of Analytical Chemistry, 11 2018, pp. 29–48.
[15] D. Weibel, S. Wong, N. Lockyer, P. Blenkinsopp, R. Hill, J.C. Vickerman, Anal. Chem. 75 (2003) 1754–1764.
[16] S. Rabbani, A.M. Barber, J.S. Fletcher, N.P. Lockyer, J.C. Vickerman, Anal. Chem. 83 (2011) 3793–3800.
[17] S.J. Lee, C.M. Choi, B.K. Min, J.Y. Baek, J.Y. Eo, M.C. Choi, Bull. Kor. Chem. Soc. 40 (2019) 877–881.
[18] T.B. Angerer, P. Blenkinsopp, J.S. Fletcher, Int. J. Mass Spectrom. 377 (2015)

591–598.
[19] S.V. Verkhoturov, S. Geng, B. Czerwiński, A.E. Young, A. Delcorte, E.A. Schweikert, J. Chem. Phys. 143 (2015) 2–7.
[20] S. Zhao, J. Xue, L. Liang, Y. Wang, S. Yan, J. Phys. Chem. C 116 (2012) 11776–11782.
[21] M. Gołuński, Z. Postawa, Acta Phys. Pol. A 132 (2017) 222–224.
[22] M. Gołuński, S.V. Verkhoturov, D.S. Verkhoturov, E.A. Schweikert, Z. Postawa, Nucl. Instrum. Methods Phys. Res., Sect. B 393 (2017) 13–16.
[23] Z.C. Xu, W.R. Zhong, Appl. Phys. Lett. 104 (2014) 261907.
[24] S.V. Verkhoturov, M. Gołuński, D.S. Verkhoturov, S. Geng, Z. Postawa, E.A. Schweikert, J. Chem. Phys. 148 (2018) 144309.
[25] O. Lehtinen, J. Kotakoski, A.V. Krasheninnikov, J. Keinonen, Nanotechnology 22 (2011) 175306.
[26] O. Lehtinen, J. Kotakoski, A.V. Krasheninnikov, A. Tolvanen, K. Nordlund, J. Keinonen, Phys. Rev. B 81 (2010) 153401.
[27] M. Kanski, D. Maciazek, Z. Postawa, C.M. Ashraf, A.C.T. van Duin, B.J. Garrison, J. Phys. Chem. Lett. 9 (2018) 359–363.
[28] R.A. Aziz, M.J. Slaman, Mol. Phys. 58 (1986) 679–697.
[29] W.D. Wilson, L.G. Haggmark, J.P. Biersack, Phys. Rev. B 15 (1977) 2458–2468.
[30] B.J. Garrison, Z. Postawa, Mass Spectrom. Rev. 27 (2008) 289–315.
[31] Z. Postawa, B. Czerwiński, M. Szewczyk, E.J. Smiley, N. Winograd, B.J. Garrison, J. Phys. Chem. B 108 (2004) 7831–7838.
[32] S. Plimpton, J. Comput. Phys. 117 (1995) 1–19.
[33] C. Anders, H.M. Urbassek, R.E. Johnson, Phys. Rev. B 70 (2004) 155404:1–6.
[34] A. Delcorte, B.J. Garrison, K. Hamraoui, Anal. Chem. 81 (2009) 6676–6686.
[35] V.N. Popok, J. Samela, K. Nordlund, E.E.B. Campbell, Phys. Rev. B 82 (2010) 201403–1 - 201403-4.
[36] W.O. Hofer, Top. Appl. Phys. 64 (1991) 15–90.
[37] W.S. Li, L. Liang, S.J. Zhao, S. Zhang, J.M. Xue, J. Appl. Phys. 114 (2013) 234304.
[38] B. Czerwinski, A. Delcorte, J. Phys. Chem. C 117 (7) (2013) 3595–3604.
[39] J. Tian, T. Zheng, J. Yang, S. Kong, J. Xue, Y. Wang, K. Nordlund, Appl. Surf. Sci. 337 (2015) 6–11.
[40] R.P. Webb, Radiat. Eff. Defects Solids 162 (2007) 567–572.
[41] M. Gołuński, Z. Postawa, J. Vac. Sci. Technol., B: Nanotechnol. Microelectron. 36 (2018) 03F112.
[42] J.H. Lee, P.E. Loya, J. Lou, E.L. Thomas, Science 346 (2014) 1092–1096.